Power System Technology **Volume 48 · Number 1 · 2024**
ISSN: 1000-3673

A Source-network Transient Interaction Modeling Method for New Power System Based on Improved Bi-LSTM Algorithm

Lü, J., Yu, J.

1. College of Resources, Shandong University of Science and Technology, Tai'an, China

2. Nanning University, Guangxi key laboratory of international join for China-ASEAN Comprehensive Transportation, Nanning, China

3. School of Traffic and Transportation Engineering, Dalian Jiaotong University, Dalian, China

ABSTRACT

In order to investigate the problem of formation collapse caused by sand leakage from segmental lining cracks, this paper selected the logical idea of the silo calculation example in PFC3D and used numerical triaxial compression to calibrate the parameters of sand particles. By simulating the changes in the contact force chain between sand particles, the bottom plate load and the porosity of the sand layer during the process of layer collapse caused by sand leakage from segmental lining cracks, the layer subsidence and sand inrush phenomena, sand flow and loss laws of the sand layer due to different openings are studied. The results show that the dynamic process of continuous formation and destruction of the soil vault leads to continuous changes in the contact force between sand particles when the segmental lining cracks cause strata subsidence. The microscopic reason for the sand intrusion disaster was that after the thickness-to-span ratio exceeded the critical value, the soil arch continued to develop towards the top surface and the top surface was connected to the opening, resulting in the inability to form a stable soil arch between the sand particles. During the loss of sand, the change in load on the bottom plate and the change in porosity at the opening corresponded to the process of destruction and formation of the soil arch. Whenever the soil arch was formed, a local peak appeared in the load curve on the bottom plate and the porosity curve at the opening. In the later stage of the sand loss process, as the loss rate increased, the frequency of soil arch formation and destruction accelerated accordingly.

1. INTRODUCTION

After years of operation in underground engineering tunnels, the concrete lining was prone to cracking to varying degrees and accompanied by water leakage, sand leakage, and other diseases. Sand and water leakage would cause varying degrees of corrosion or damage to the power, communications, and other equipment in the tunnel, which would affect driving safety. At present, laboratory test, physical model and numerical simulation are the main research methods to study the strata subsidence caused by lining fracture leakage [1, 3, 6-7]. Zheng et al. [19] created a visual simulation experimental equipment for water-sand leakage that can

adjust the gap width and pointed out that after the gap width exceeds the critical value, a large amount of soil would be lost. The process of water-sand leakage was a dynamic process of the ongoing formation and destruction of soil arch. Liang et al. [11] found that the water-sand inrush process was a process of continuous redistribution of soil stress, the continuous development of sand cracks eventually penetrates the entire sand layer by using the test device of water and sand inrush in loose coal seams. Based on the incipient sediment theory, Wu and Lu [17] studied the load of soil particles when the sand inrush phenomenon happened, established a physical and mechanical model of sand inrush structure, and proposed the theoretical expressions for the condition under which sand inrush occurred. Jiang et al. [8] carried out numerical biaxial compression tests on sandy by using PFC particle flow software and analyzed the effect of the anti-rotational properties of the particles on the material yield of the sandy. Zhou et al. [20] chose the PFC particle flow code to adjust the particle position according to the contact force and analyzed the effect of the meso-parameter on the failure forms of the slope. Chang et al. [4] based on field investigations and laboratory tests, the detailed identification of mesoscopic parameter was calibrated, and a PFC2D model was established. Liu et al. [13] selected PFC3D particle flow software to build a numerical simulation model considering the cohesion between particles and the constitutive relationship and studied the stress path of different specimens after loading. Ding and Zhang [18] created a new contact model which properly considers the contribution of moments to normal and shear contact stresses and the condition at which the contact fails was proposed and implemented in the three-dimensional Particle Flow Code (PFC3D). Lian et al. [10] used the Particle Flow Code to simulate the discontinuous deformation of strata, especially the cracks caused by underground coal mining. Bai et al. [2] used PFC2D particle flow software to simulate the caving of the top-coal in the stope and concluded that the process of top-coal release was a continuous evolution of contact force arch formation and destruction. Koyama and Jing [9] used PFC2D particle flow software to establish rock samples and conducted numerical biaxial compression tests to simulate the compressive strength of rocks under different particle sizes and sample sizes. The results show that when the particle size and the sample size were greater than the critical value, the influence of particle dimension on rock strength can be ignored. Fakhimi and Gharahbagh [5] used the discrete element approach to alter the hole parameters and analyzed the rock mechanical parameters and deformation characteristics with various hole sizes and porosities. Chen et al. [15] built the model to use discrete component software, as a two-dimensional particle flow program. The use of PFC particle flow software could better simulate the problem of sand loss in underground engineering and obtain phenomena and results consistent with indoor experiments. This paper used PFC3D particle flow software to carry out numerical simulations to study the flow law and mechanism of sand particles in order to deepen the knowledge and understanding of sand inrush and subsidence hazards caused by sand leakage from lining cracks.

2. SOIL SAMPLES AND MECHANICAL PARAMETERS

2.1. Soil samples of numerical simulation

In this experiment, sand with a framework particle size of 0.076mm~2mm was selected as the experiment soil samples. The gradation curve was shown in Figure 1.

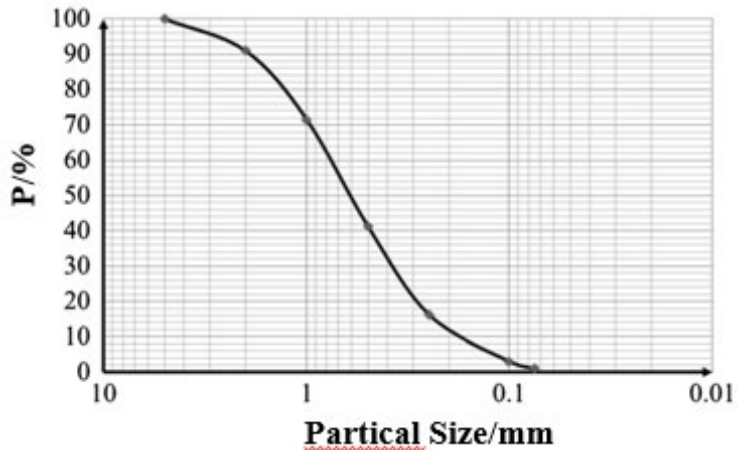

Figure 1. The soil sample's gradation curve

2.2. The primary numerical parameters of soil samples (Table 1)

Table 1 Macroscopic parameters of the experiment soil sample

Parameter	Modulus of elasticity/ E/Mpa	Bulk density /γ/KN.m^3	Internal friction angle/ φ/°	Cohesion c/KN.m^3	Porosity ratio/ e	Relative density/ GS
Experiment sand value	20.5	15.5	31	0	0.72	2.65

3. NUMERICAL SIMULATION OF STRATA SUBSIDENCE

3.1. Parameter calibration of the model

Prior to the simulation experiment of this study, parameter calibration was carried out to determine the key parameters of the parameters of the particle group and the linear contact group. The stress-strain curves under the numerical simulation were obtained by triaxial compression experiment, and the normal stiffness, tangential stiffness, tangential stiffness and coefficient of friction were continuously adjusted to fit and compared with the actual stress-strain curves of the sand particles. The three key mesoscopic parameters of normal stiffness, tangential stiffness, tangential stiffness and friction coefficient for the fine sand particles in this study [14]. The triaxial compression model was shown in Figure 2.

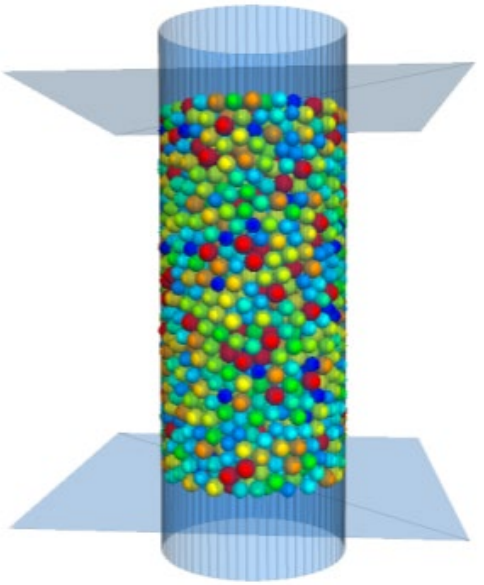

a. Front view

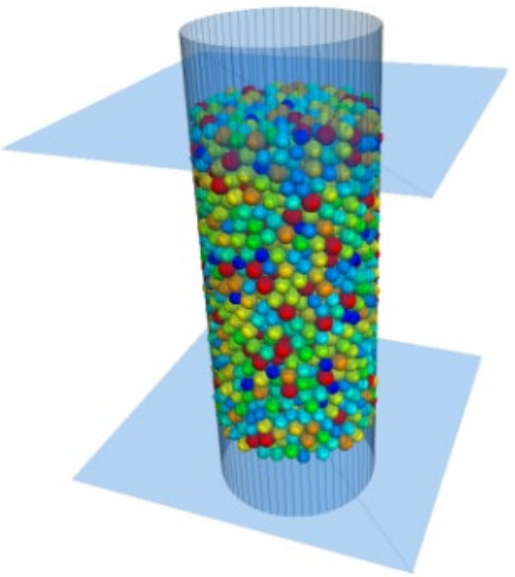

b. Side view

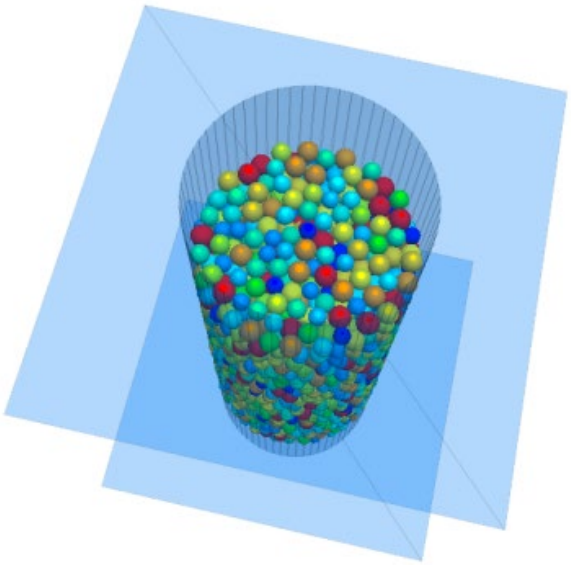

c. Top view

Figure 2. Structural drawing of triaxial compression wall

In PFC, the wall could not be stressed, so the stress could only be converted into velocity applied to the cylindrical sidewall and the upper and lower walls [16]. During the whole loading process, the velocity of the lateral restraint was adjusted to keep the restraint stress constant by a numerical servo mechanism, which was performed by calling the FISH functions servo and "get_gain" once per cycle. The "get_ss" function was also called to determine the stress, and the numerical servo control was used to adjust the restraint velocity to reduce the difference between the measured stress and the required stress.

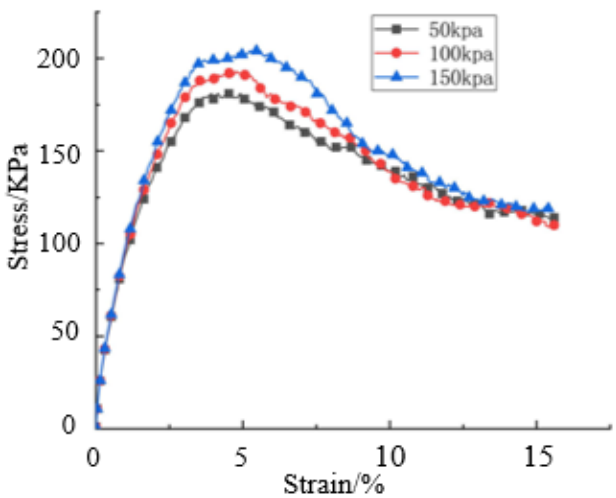

Figure 3. Stress-strain curve

Due to the unique nature of sand particles, a cyclic loading method was used for this experiment. After the 3D model specimen was loaded to 80% of the peak strength, the load was reapplied to the upper and lower walls. The servo system was used to keep the cylindrical wall confining pressure steady, with values of 50 KPa, 100 KPa, and 150 KPa, respectively, and a velocity of 5e-3 m/s for the upper and lower walls. The final stress-strain curve obtained conforms to the plastic characteristics of the sand selected for this experiment and approximates the axial stress and axial strain curves of the fine sand particles actually used, as shown in Figure 3. By plotting the Moore circle, the angle of internal friction of the selected sandy soil was obtained as 32.3°, with a relative error of 3.05% [12]. The specific microscopic parameters of the fine sand particles and the wall were shown in Table 2.

Table 2. Microscopic parameters table of sand particle and wall

Material	**Diameter R/mm**	**Density ρ/kg·m^{-3}**	**Normal stiffness Kn/N·m^{-1}**	**Tangential stiffness Ks/N·m^{-1}**	**Friction μ**
Particle	5～11	2750	1.0e7	1.0e7	0.65
Wall	—	—	1.0e8	1.0e8	0.15

In the simulation calculation, if the radius of the sphere were set according to the actual size of the sand particles, the calculation time would be greatly increased. The amount of calculation would exceed the computer's calculation capacity, which would not only cause the simulation results to converge slowly but even cause the consequences of not being able to calculate. Therefore, after several adjustments, the radius of the sand particles in the model was set to 3mm~5mm.

3.2. Establishment of numerical simulation model

In this study, the cylindrical wall was first constructed in PFC3D to form a topless, bottomless cylindrical structure with a cross-sectional circular radius of 0.275m and a height of 0.8m. Four trapezoidal walls were used to form the bottom plate of the sand leakage cylinder, forming a rectangular opening, and the particles were generated in the cylindrical area enclosed by the wall in accordance with the chosen fine sand gradation and brought to a stable state under gravity. The rectangular wall in the center of the bottom plate was then removed to simulate rectangular cracks in the segmental lining, as shown in Figure 4.

This study only simulated the subsidence and sand inrush process of "dry sand". Focus on the study of morphologic change, contact force chain change, the bottom panel load change law, the porosity of the sand layer above the opening change law during the sand loss process, and the impact of thickness-to-span ratio on sand loss. The auxiliary tool PFC2D was used to display the sand particle loss process and the change in the contact force chain. The sand leakage effect of the three-dimensional numerical model is shown in Figure 5.

a. Model front view

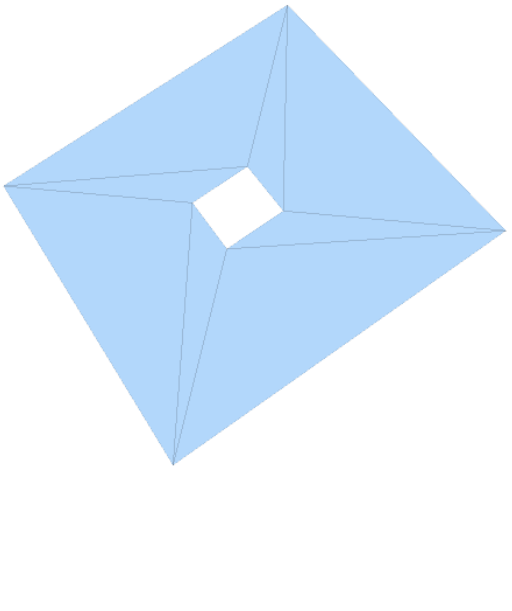

b. Numerical model of bottom rectangular opening

Figure 4. Numerical simulation model

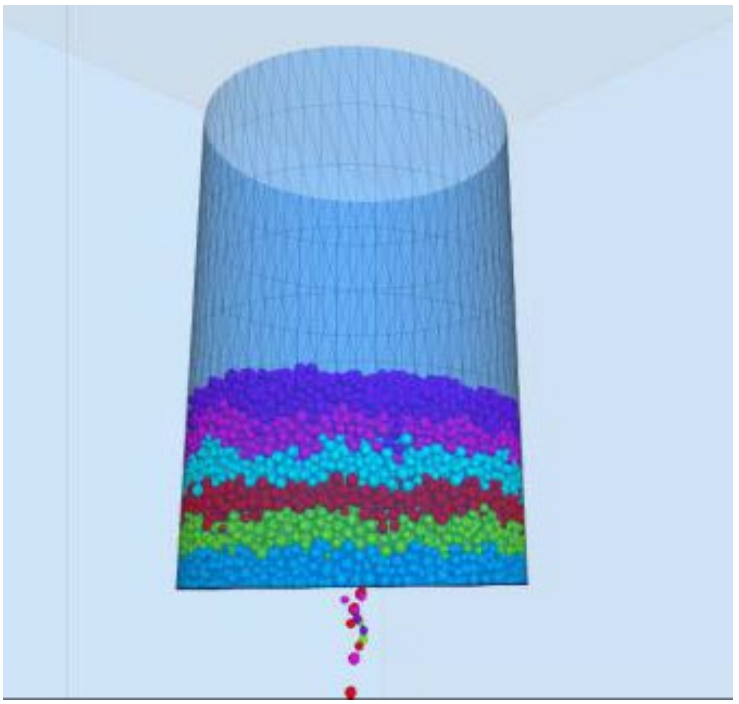

a. Sand leakage effect diagram of 3D numerical model

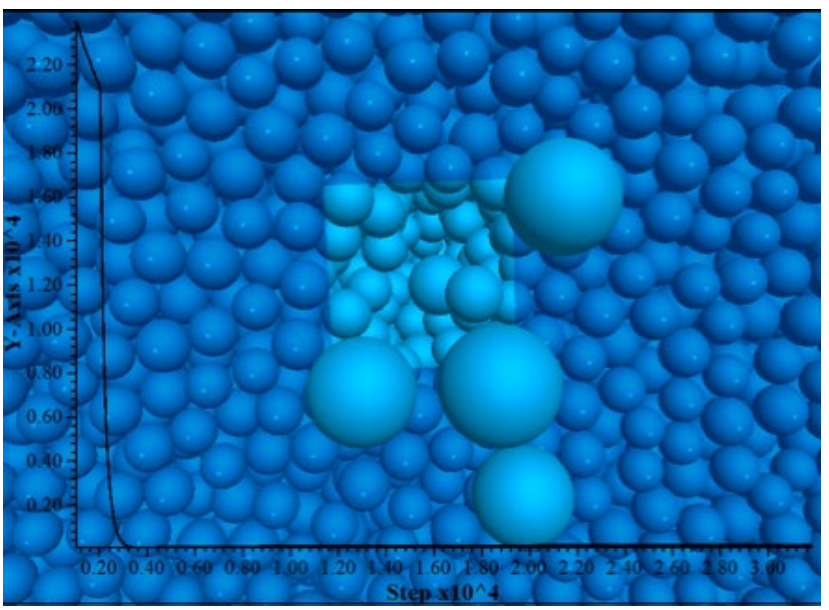

b. Effect picture of particles leaking at the bottom

Figure 5. Effect picture of sand leakage in three-dimensional numerical model

4. ANALYSIS OF NUMERICAL SIMULATION RESULTS

4.1. Change in flow morphologic and contact force chain in sand body

Taking a rectangular opening of 30mm×30mmas an example, input the mesoscopic parameters in table 2 into the program, and generated the height of 300mm particle layer, the porosity of the particle was set to 0.25. Soil particles were stratified at 100mm intervals, after applying gravity through the calculation cycle to set the velocity of the particles to zero, then opened the rectangular opening of the bottom panel to make the particles fall under the action of gravity.

4.1.1. Sand body flow morphologic

The numerical simulation experiment of the deformation process of the sand layer loss was shown in Figure 6. When the sand leakage started, the sand particles near the opening first leaked out and formed a damaged surface at the bottom of the soil body. With the loss of sand, the damaged surface continued to spread to the top of the soil body, creating a vertical subsidence area. As the loss of sand increased, the soil on both sides of the vertical subsidence area could not maintain stability, constantly slid to the opening, and the funnel-shaped collapse area was formed. Subsequently, the follow-up area sand outside the collapse area slid to the opening and eventually stabilized due to internal cohesion and particle friction.

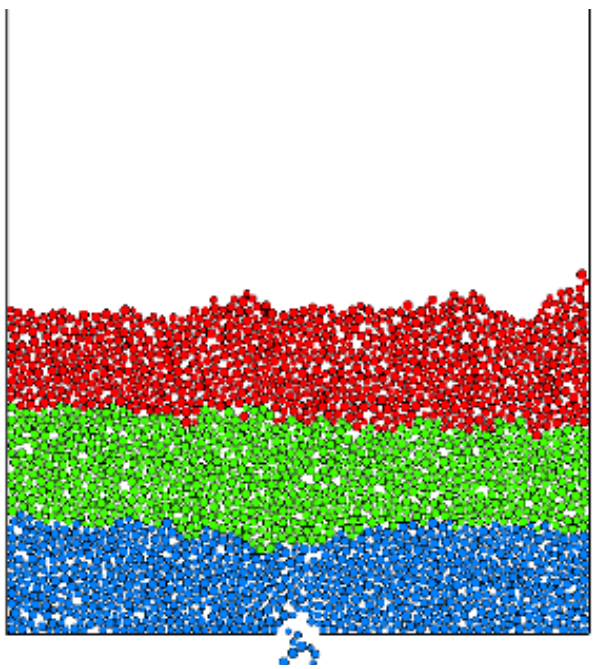

a. The Initial State

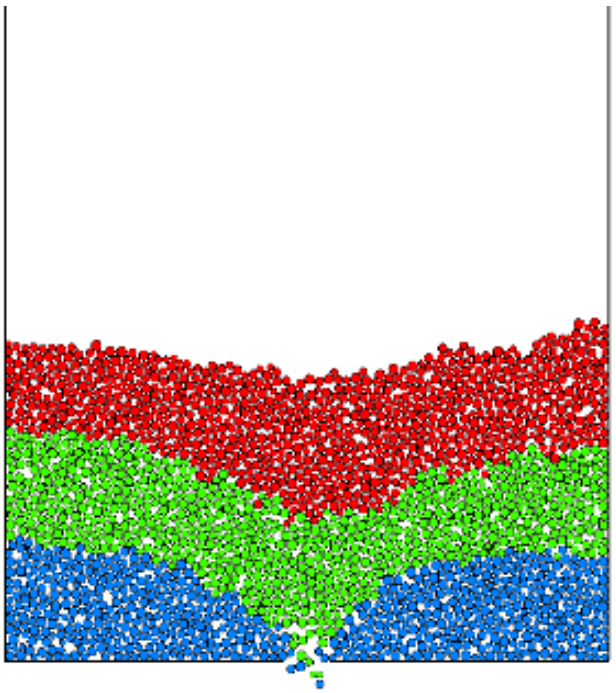

b. 600000 steps

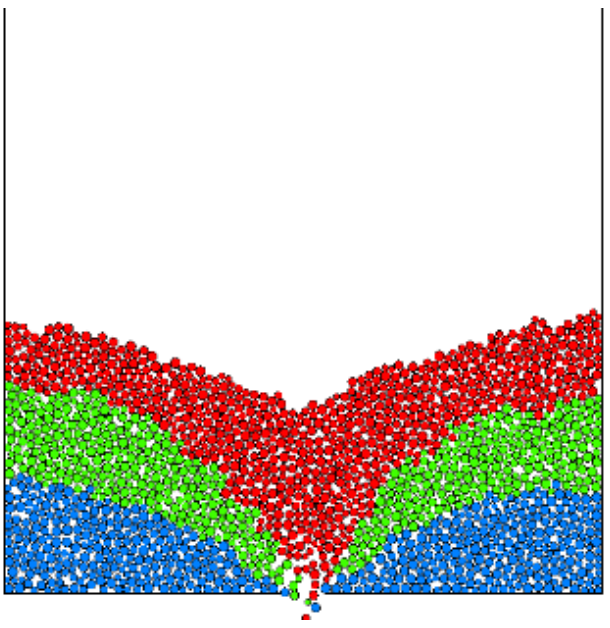

c. 1200000steps

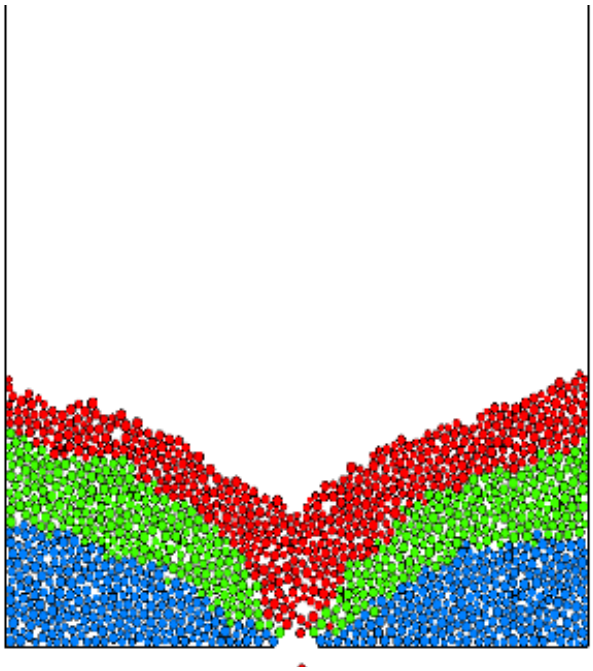

d. 2000000 steps

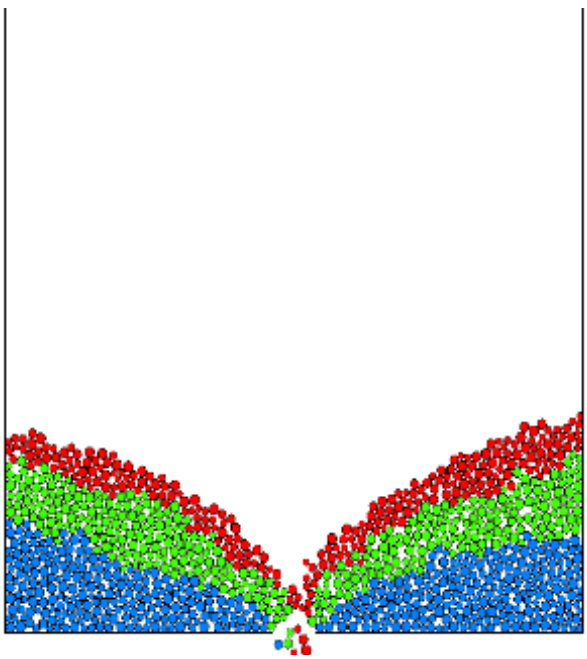

e. 2500000 steps

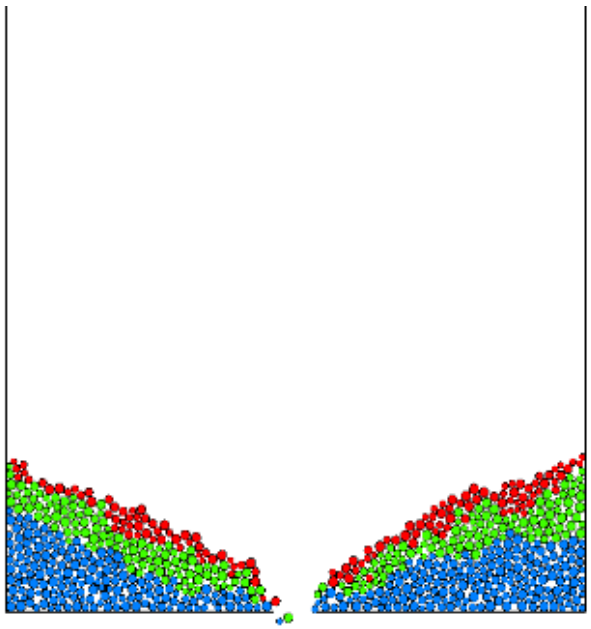

f. 3400000 steps

Figure 6. The deformation process of sand layer loss

4.1.2. Change in contact force chain

Figure 7 showed the change in the contact force chain during the sand loss process. The size of the contact force was represented by the thickness of the cylinder, the thicker the cylinder, the stronger the contact force between the two particles. The thinner the cylinder, the weaker the contact force between the two particles. It can be seen from Figure 7 that in the initial state, the contact force between the lower sand particles was relatively larger than the contact force between the upper sand particles. A small force arch was quickly formed around the opening when the sand started to leak out. Because it was not enough to support the overlying sand layer, it quickly ruptured, and the sand slid toward the opening to form a new force arch. With the continuous loss of sand, the force arch gradually developed toward the top surface until it penetrated the opening and the top surface of the sand layer. It was showed that sand loss was a process of continuous formation and destruction of soil arch between sand particles.

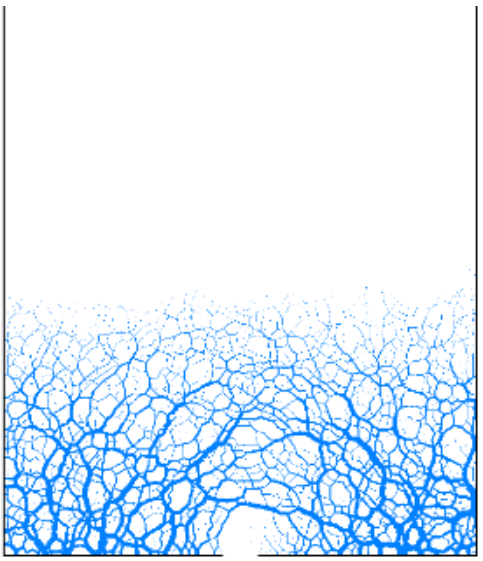

a. The Initial State

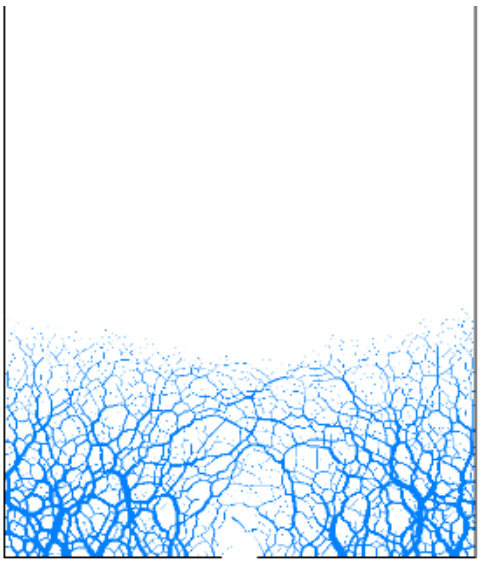

b. 600000 steps

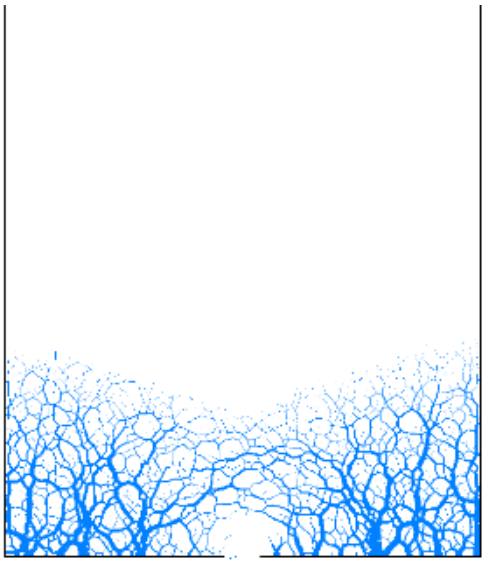

c.1200000 steps

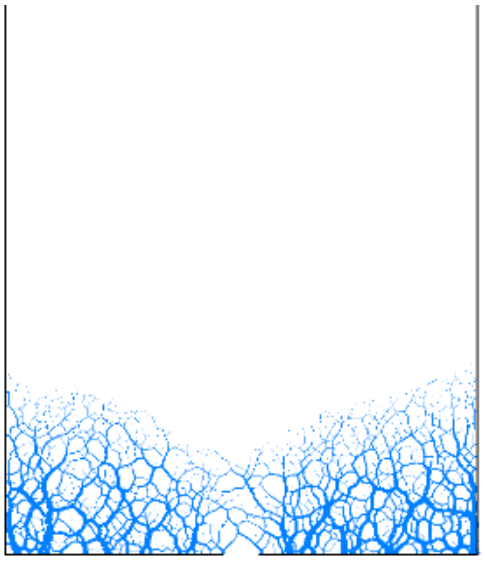

d. 2000000 steps

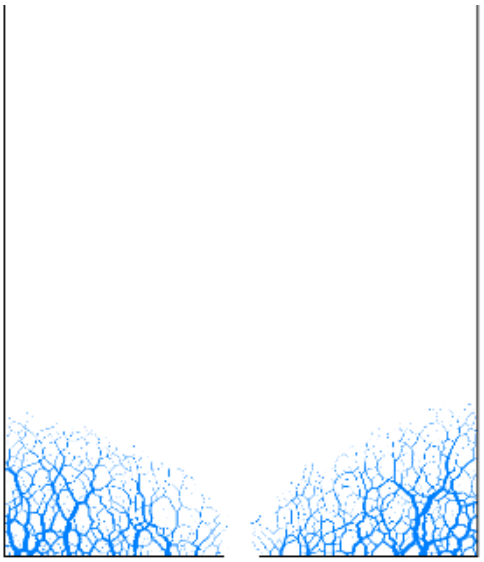

e. 2500000 steps

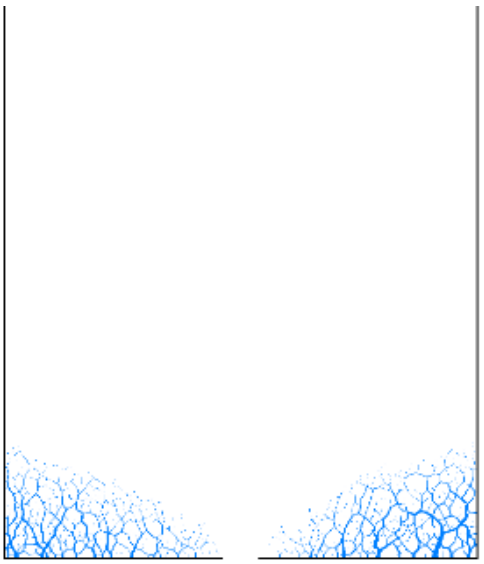

f. 3400000 steps

Figure 7. Development of contact force chain during sand leakage

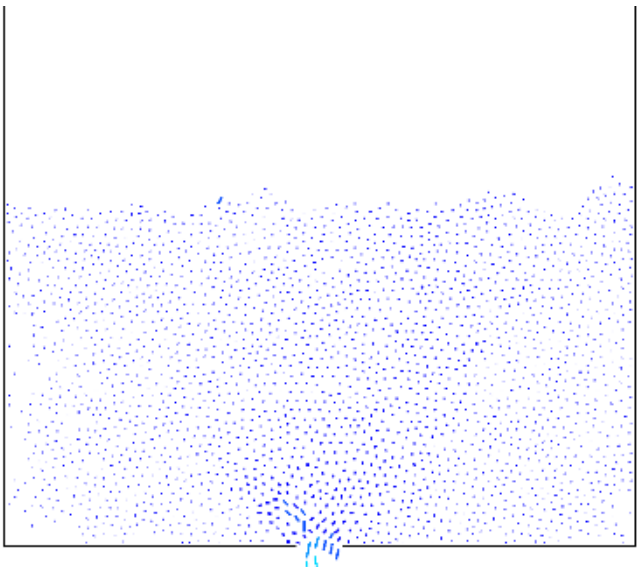

a. The Initial State

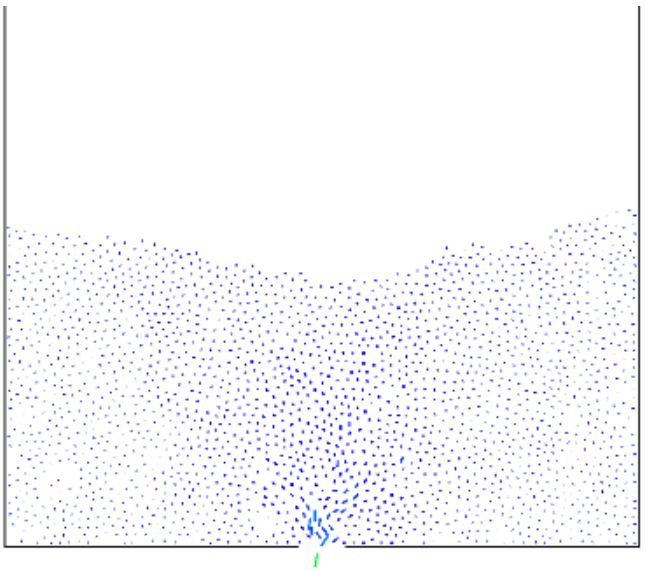

b. 600000 steps

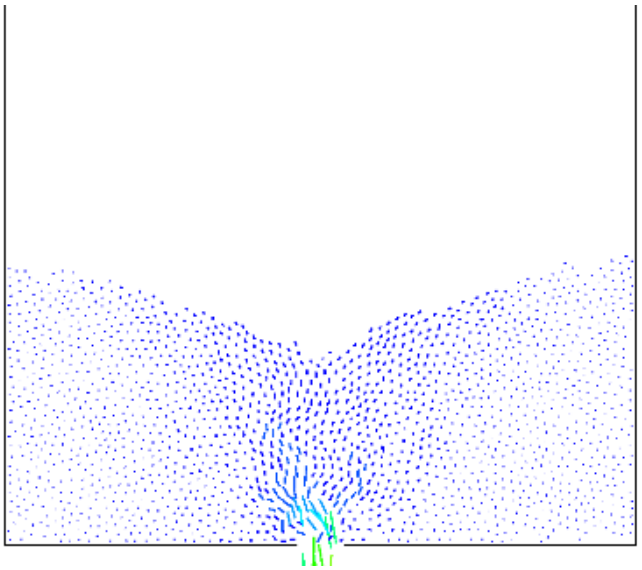

c.1200000 steps

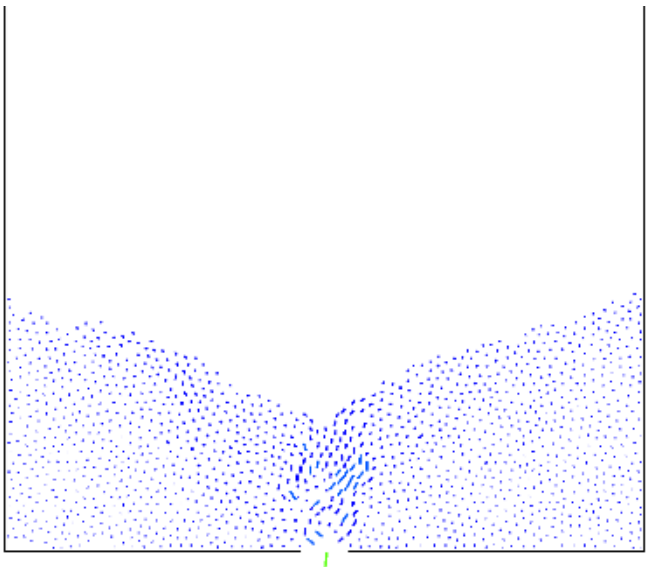

d. 2000000 steps

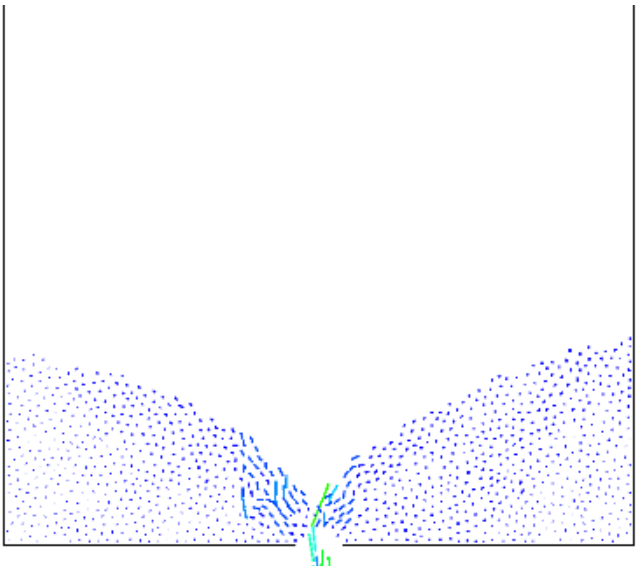

e. 2500000 steps

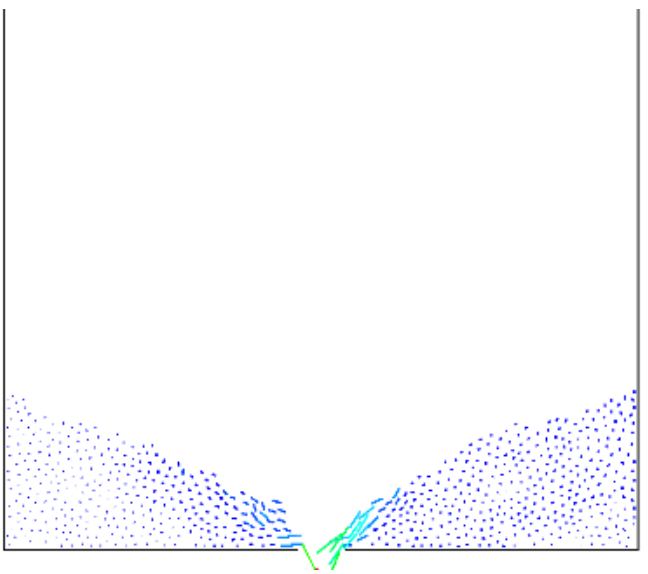

f. 3400000 steps

Figure 8. Velocity vector diagram of sand loss process

4.2. Change of sand particle velocity vector

Considering the process of sand leakage with a 30mm×30mm opening and the soil thickness of 300mm as an example. The change in sand particle velocity during the process of sand loss are shown in Figure 8. The green part in the figure was larger than the blue part of the sand particle loss velocity. In the process of sand loss, the horizontal velocity of sand particles mainly occurred in a small area on both sides of the opening. The horizontal velocity in the vertical subsidence area was very small and can basically be ignored. After the funnel-shaped collapsed surface was formed, the horizontal velocity of sand particles in the sand layer on both sides of the funnel surface showed the characteristics of layering from the outside to the inside. The moving velocity of sand particles on the surface layer was high, and the inside of the sand layer gradually decreased until it stopped.

4.3. Influence of thickness-to-span ratio on sand loss process

In order to investigate the influence of the thickness-to-span ratio on the sand loss process when the thickness of the soil layer was fixed, the numerical simulation experiment plan was designed as in Table 3, and the simulation results was shown in Figure 9.

Table 3. Numerical simulation experiment table of thickness-to-span ratio

Adjacent to both sides L1×L2/mm	30×14	30×18	30×22	30×30	35×35
Diagonal length of rectangular opening/mm	33.1	35	37.2	42.43	50
thickness-to-span ratio	6	5.7	5.4	4.7	4
Sand thickness/mm	200	200	200	200	200

As shown in Figure 9, in the thickness-to-span ratio for 6.0, 5.7, 5.4 of the simulation results appeared in the opening of the sand particles blocked into the arch phenomenon, and in the thickness-to-span ratio for 4.7 and 4, the opening of the sand particles did not appear blocked into the arch phenomenon. It can be considered that when the thickness-to-span ratio of the sand layer was a fixed value of 200 mm, the critical thickness-to-span ratio of the sand layer was 5.4.

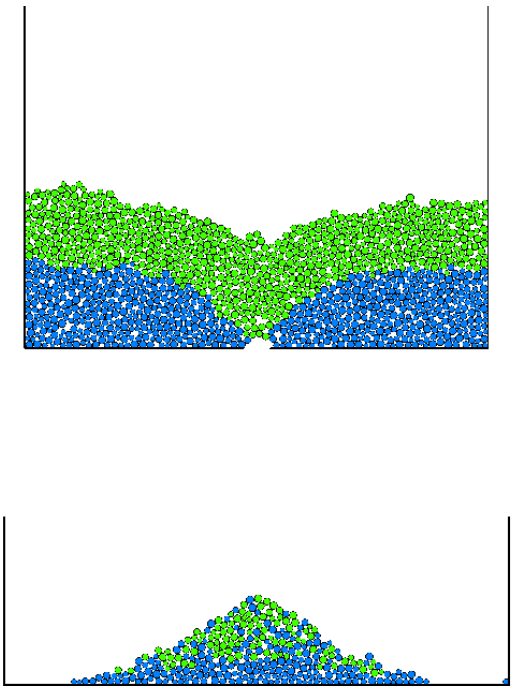

a. The thickness-to-span ratio is 6

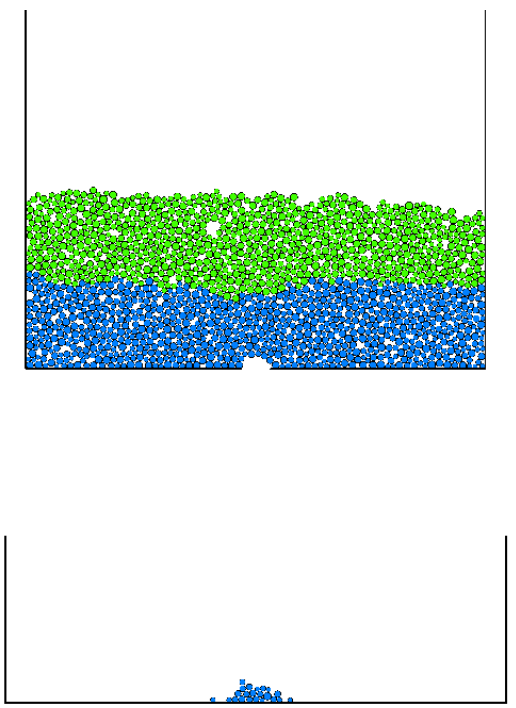

b. The thickness-to-span ratio is 5.7

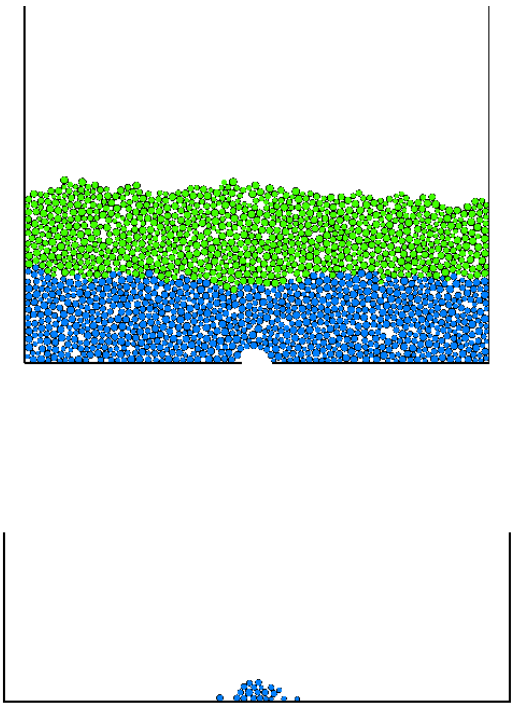

c. The thickness-to-span ratio is 5.4

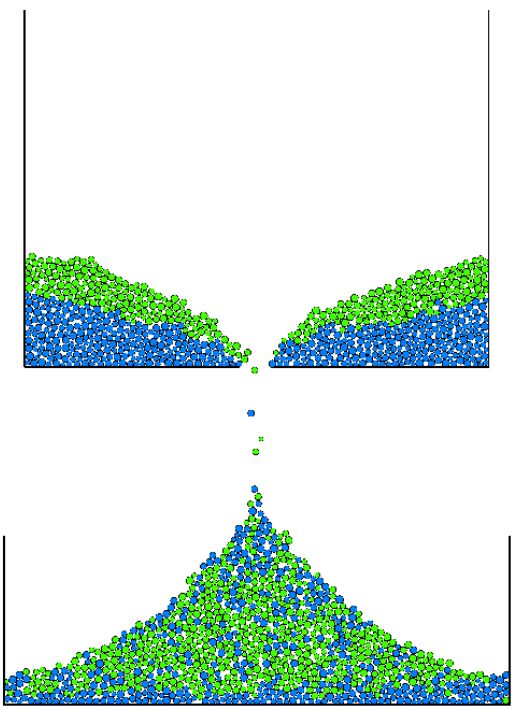

d. The thickness-to-span ratio is 4.7

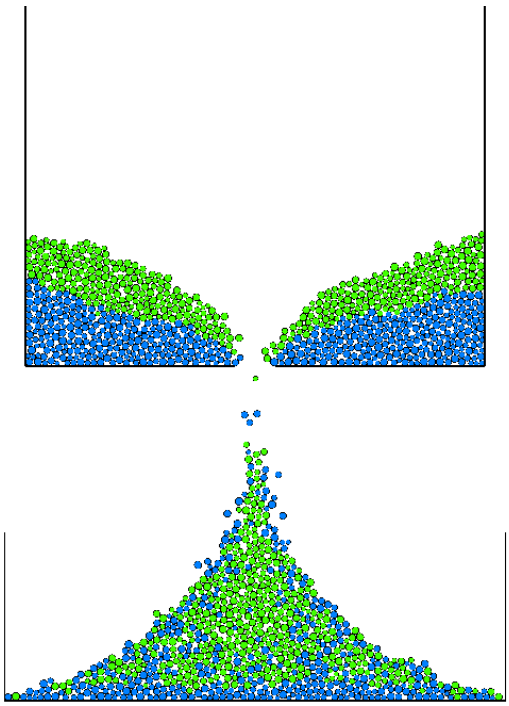

e. The thickness-to-span ratio is 4

Figure 9. Numerical simulation results for different thickness-to-span ratios

4.4. Change in load on the bottom panel of sand leakage cylinder

According to the numerical simulation experiment plan designed in Table 3, the load on the bottom plate was monitored, as shown in Figure 10.

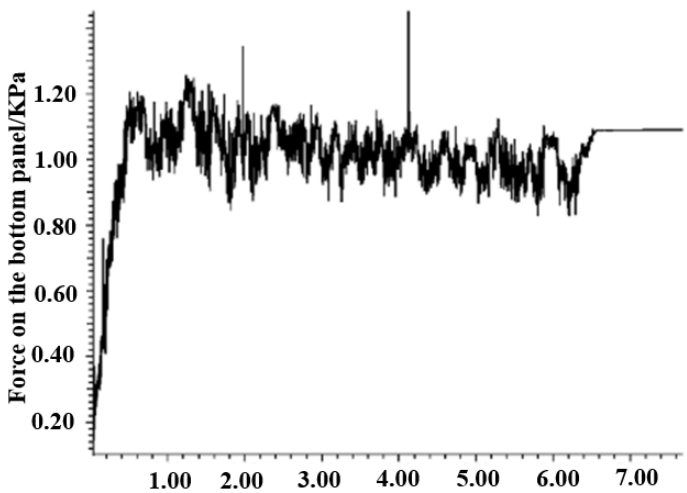

a. The thickness-to-span ratio is 6

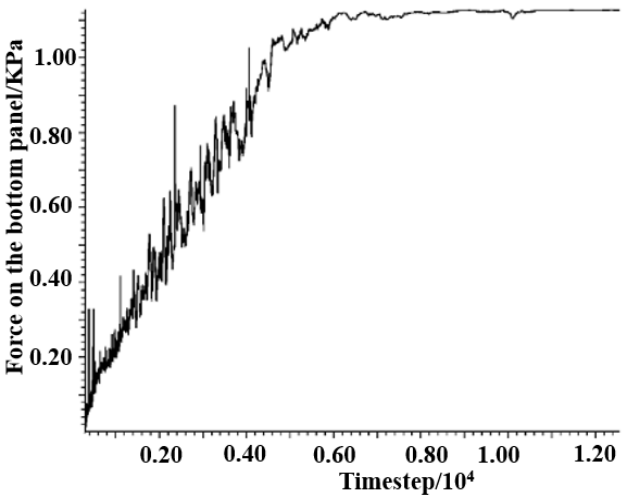

b. The thickness-to-span ratio is 5.7

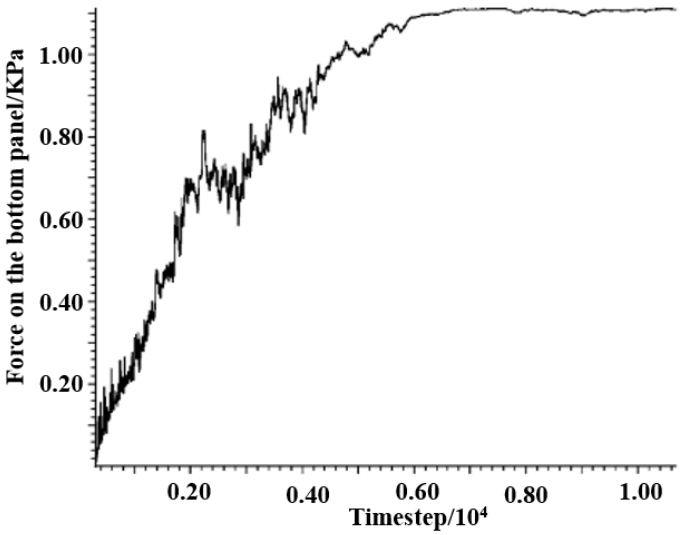

c. The thickness-to-span ratio is 5.4

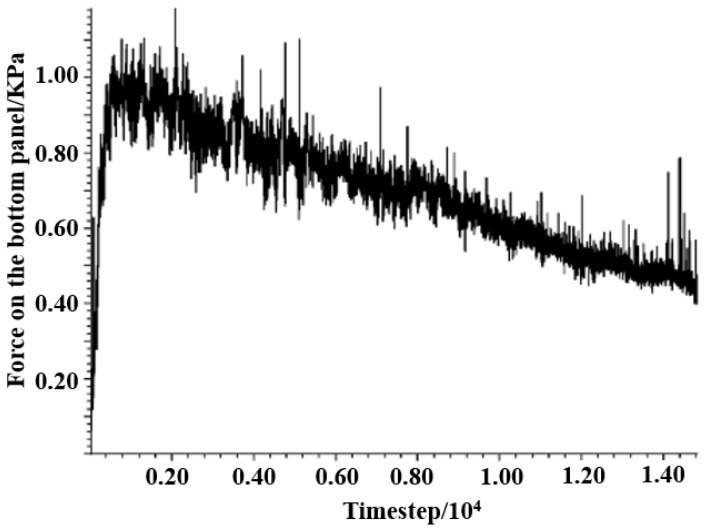

d. The thickness-to-span ratio is 4.7

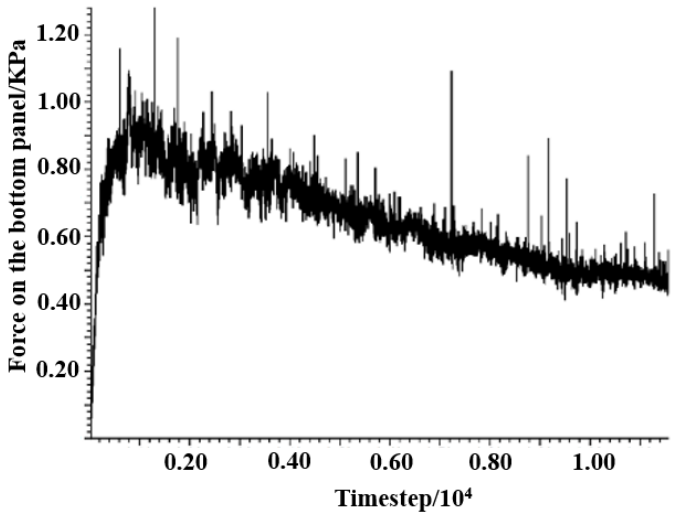

e. The thickness-to-span ratio is 4

Figure 10 The change of load on the bottom panel when the thickness-to- span ratio are 4~6

It can be seen from Figure 10 that when the sand loss started, the load on the bottom panel increased suddenly. As the sand particles continued to flow out, the load on the bottom plate also fluctuated. When a new soil arch was formed around the opening, the load on the bottom panel would appear a phased peak, which corresponded to the process of soil arch destructing and then forming. For the numerical simulation experiments with thickness-to-span ratios of 6, 5.7, and 5.4, since the sand layer finally formed a stable soil arch, the load curve of the bottom panel in the early stage of the numerical operation fluctuated sharply and finally tended to stabilize. Comparing the numerical simulation experiments with a thickness-to-span ratio

of 4.7 and 4, the bottom panel load also suddenly increased at the beginning of the sand loss, but with the sand continued to be lost, the soil arch continued to form and destruct. As a stable soil arch capable of supporting the weight of the overlying sand was never formed, the load on the bottom plate was constantly reduced.

4.5. Change of the porosity near the opening

According to the numerical simulation experiment plan designed in Table 3, the porosity of the sandy soil layer near the opening was monitored, as shown in Figure 11.

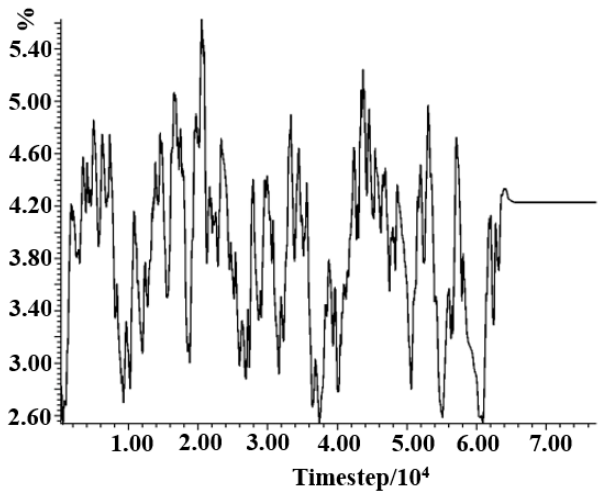

a. The thickness-to-span ratio is 6

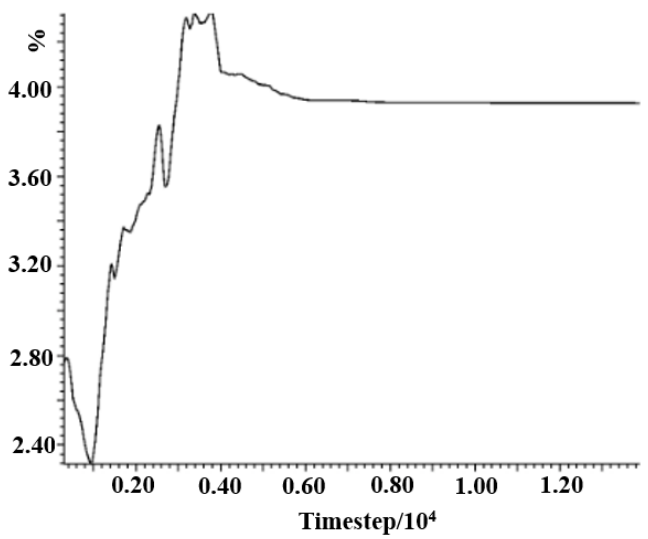

b. The thickness-to-span ratio is 5.7

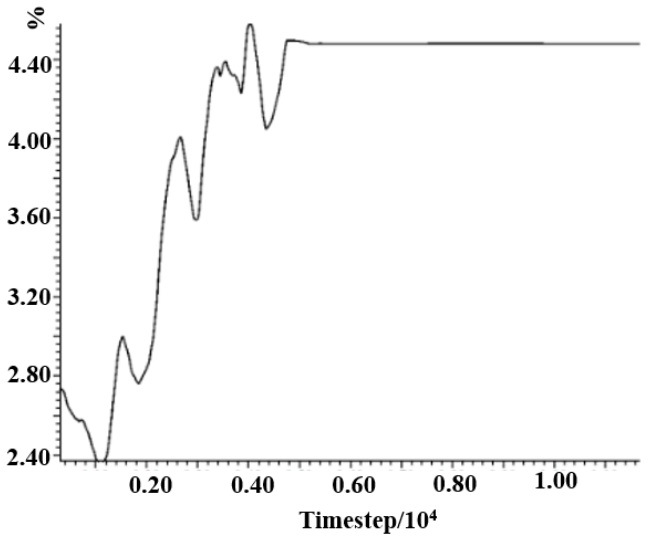

c. The thickness-to-span ratio is 5.4

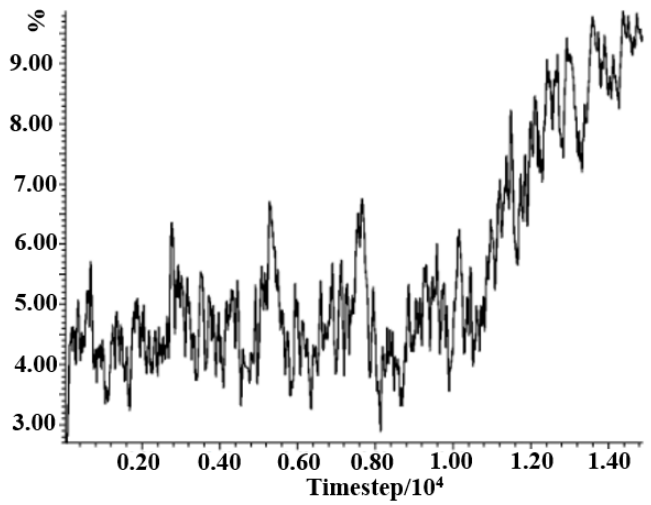

d. The thickness-to-span ratio is 4.7

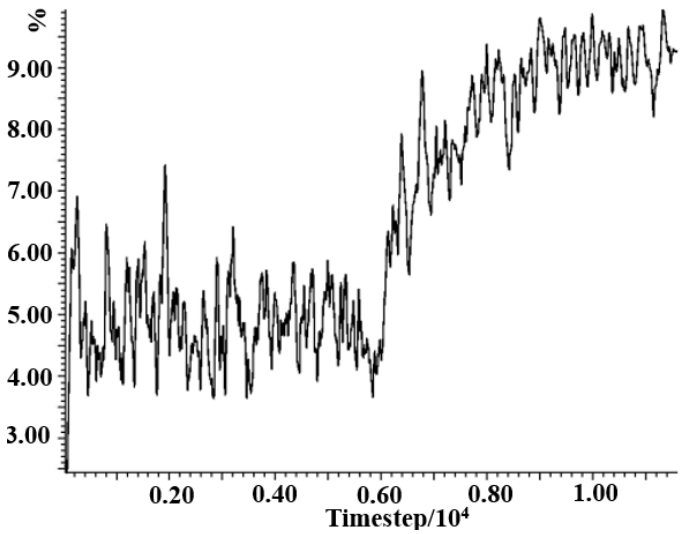

e. The thickness-to-span ratio is 4

Figure 11 The porosity of sand layer at the opening when the thickness-to-span ratio are 4~6

Figure 11 showed that when the sand began to lose, the sand near the opening suddenly leaked out, leading to a sudden decrease in porosity. Subsequently, the sand near the opening began to surge to the opening, leading to a rapid increase in porosity. With the continuous loss of sand, the soil arch near the opening continued to form and destruct, causing the porosity curve to fluctuate constantly. Comparing the porosity of the sand layer at the different openings can be known, when the thickness-to-span ratio exceeded the critical value, the sand layer would not produce the sand inrush, and eventually formed a stable soil arch, so the porosity near the opening would maintain when it changed to a certain value. When the thickness-to-span ratio fell below the critical value, the sand layer would produce sand inrush until a stable funnel-shaped subsidence surface formed, so the porosity near the opening was constantly increasing.

5. CONCLUSION

1) When the sand layer began to be lost, the soil bow would quickly form near the opening. With the continuous loss of sand, the contact force between sand particles would continue to change, and the soil arch would continue to form and destroy, gradually extending from the vicinity of the opening to the top surface of the sand body. Therefore, the mesoscopic reason for the sand inrush disaster was that after the thickness-to-span ratio exceeded the critical, the soil arch continued to develop toward the top surface, the top surface and the opening were connected, and a stable soil arch could not form between sand particles.
2) In the sand loss process, sand particles mainly produced a vertical flow direction, and the horizontal velocity mainly occurred in a small area on both sides of the opening. In the vertical subsidence area, horizontal velocity was very small, which can basically be ignored.

3) The change of load on the bottom plate and the change of porosity at the opening corresponded to the formation and destruction process of the force arch. In the process of sand loss, whenever the soil arch was formed, a local peak appeared in the load curve on the bottom panel and the porosity curve at the opening. With the continuous loss of sand, the fluctuation of the bottom panel load curve and porosity curve became more and more violent. In the later stage of the sand loss process, the loss velocity of sand increased, and the frequency of soil vault formation and destruction accelerated accordingly.

REFERENCES

[1] Bi, Z.W., "Analysis on ground behavior law of shallow coal seam based on PFC2D", Mining Safety & Environmental Protection, 2013, 40(03): p. 43-46.

[2] Bai, Q.S., Tu, S.H., Wang, C., "Numerical simulation on top-coal arching mechanism", Journal of Mining & Safety Engineering, 2014, 31 (2): p. 208-213.

[3] Cao, J., Huang, Q.X., Guo, L.F., "Subsidence prediction of overburden strata and ground surface in shallow coal seam mining", Scientific Reports, 2021, 11(1): p. 18972.

[4] Chang, C., Bo, J., Qi, W., Qiao, F., & Peng, D., "Study on instability and damage of a loess slope under strong ground motion by numerical simulation", Soil Dynamics and Earthquake Engineering, 2022, 152: p. 107050.

[5] Fakhimi, A., & Gharahbagh, E. A., "Discrete element analysis of the effect of pore size and pore distribution on the mechanical behavior of rock", International Journal of Rock Mechanics and Mining Sciences, 2011, 48(1): p. 77-85.

[6] Guo, T.T., "Study on calculation methods of soil pressure of the culvert under high fill", Industrial Construction, 2010, 40(S1):p. 729-731.

[7] Han, G., Qi, Q.J., Cui, T.J., Wang, L.G., "Mining plan simulation and rock migration analysis in steep seam mining", Journal of Mining & Safety Engineering, 2016, 33(04):p. 618-623+629.

[8] Jiang, M.J., Li, X.M., Sun, Y.G., Hu, H.J., "Discrete element simulation of biaxial compression test considering rolling resistance", Rock and Soil Mechanics, 2009, 30(S2): p. 514-517.

[9] Koyama, T., & Jing, L., "Effects of model scale and particle size on micro-mechanical properties and failure processes of rocks-A particle mechanics approach", Engineering Analysis with Boundary Elements, 2007, 31(5):p. 458-472.

[10] Lian, X., Zhang, Y., Liu, J., Deng, W., Guo, J., & Cai, Y., "Rules of overburden crack development in coal mining with different ratios of rock-soil strata conditions", Arabian Journal of Geosciences, 2022, 15(6): p. 511.

[11] Liang, Y., Tan, Z.D., Li, G.J., "Simulation test research on water and soil outbursts of weak binding soil", Journal of Chang'an University (Natural Science Edition), 1996, (1): p. 19-22.

[12] Liu, Y.Q., Zhou, H.W., Li, Y.H., Yi, H.Y., Xue, D.J., “Water-sand inrush simulation under shallow coal mining based on the particle flow code”, Journal of Xi'an University of Science and Technology, 2015, 35(5): p. 534-540.

[13] Liu, Y., Zhu, J.M., Yan, B., “Meso-mechanical simulation study on triaxial test of coarse-grained soil based on DEM”, Journal of Railway Science and Engineering, 2014, 11(4): p. 58-62.

[14] Luo, Y., Gong, X.N., Wu, R.Q., “Analysis and simulation of fluid-particles interaction with particle flow code”, Journal of Zhejiang University (Engineering Science), 2007, 41(11): p. 1932-1936.

[15] Chen, S., Xia, Z., Feng, F., “Numerical Simulation of Strength, Deformation, and Failure Characteristics of Rock with Fissure Hole Defect”, Advances in Materials Science and Engineering, 2020, 2020: p. 7048645.

[16] Sun, H.X., Zhao, W., Wang, Z.Y., “Monitoring and numerical simulation of underground pipeline settlement during shield tunneling construction”, Journal of Shenyang University of Technology, 2010, 32(4): p. 454-458.

[17] Wu, Y.P., Lu, M.S., “Analysis of sand inrush generation condition in coal mining of shallow coal seam”, Journal of Mining & Safety Engineering, 2004, 20(3): p. 57-58+61-118.

[18] Ding, X., & Zhang, L., “A new contact model to improve the simulated ratio of unconfined compressive strength to tensile strength in bonded particle models”, International Journal of Rock Mechanics and Mining Sciences, 2014, 69: p. 111-119.

[19] Zheng, G., Dai, X., Zhang, X.S., “Experimental study and numerical simulation of leaking process of sand and water in underground engineering”, Chinese Journal of Rock Mechanics and Engineering, 2014, 33(12): p. 2458-2471.

[20] Zhou, J., Wang, J.Q., Zeng, Y., Zhang, J., “Simulation of slope stability analysis by particle flow code”, Rock and Soil Mechanics, 2009, 30(1): p. 86-90.